Multistability formation and synchronization loss in coupled Hénon maps: Two sides of the single bifurcational mechanism

V. Astakhov and A. Shabunin
Department of Physics, Saratov State University, Astrakhanskaya 83, 410071 Saratov, Russia

W. Uhm and S. Kim
Nonlinear and Complex Systems Laboratory, NRL, Department of Physics, Pohang University of Science and Technology, Pohang, 790-784 Korea

(Received 11 October 2000; published 20 April 2001)

We investigate phenomena of multistability and complete chaos synchronization in coupled Hénon maps, which is an invertible system. Multiparametric analysis of a selected family of periodic orbits for coupled Henon maps shows that a single bifurcational mechanism describes both a loss of chaos synchronization and multistability formation. The process of bubbling transition and riddle basins, and the multistability formation in invertible systems are described in detail.

DOI: 10.1103/PhysRevE.63.056212 PACS number(s): 05.45.−a

I. INTRODUCTION

Recently chaotic synchronization has been a subject of active research. Though there is still no common view on the phenomenon of chaotic synchronization, one of the widely studied ones includes ''complete synchronization,'' when oscillations of subsystems are equal or nearly equal to each other at every moment in time [1,2]. A large number of works have been devoted to the study of general bifurcational mechanisms which lead to the loss of complete chaotic synchronization [3–11].

As is known in the case of complete synchronization in a system of symmetrically coupled identical oscillators the chaotic attractor is located at the symmetric subspace $\mathbf{x}_1=\mathbf{x}_2$ ($\mathbf{x}_{1,2}$ are dynamical variables of the subsystems) of the whole phase space of the system. The existence of this subspace is determined by the invariance of the system under the exchange of $\mathbf{x}_1 \leftrightarrow \mathbf{x}_2$. A possibility of realization of the synchronous regimes in real experiments is determined by the stability of the limit set in the symmetric subspace to the transversal perturbations, i.e., by the sign of the normal Lyapunov exponent. When all normal Lyapunov exponents on the attractor are negative, but a normal exponent on some limit sets embedded in the attractor are positive. In this case, it was shown that a synchronous chaotic regime exists. This, however, is not robust [12,11]. Any small noise and any small mismatch between parameters of the subsystems lead to the so-called bubbling behavior [7] when the difference $\|\mathbf{x}_1-\mathbf{x}_2\|$ looks similar to the on-off intermittency. The transition to the bubbling behavior can be the first step to the destruction of the chaotic synchronization regime.

In Refs. [10,11] the bifurcational mechanism of the destruction of the regime of synchronous chaos was considered in detail for a system of symmetrically coupled logistic maps. It was shown that the transition from robust synchronous chaos to bubbling behavior is caused by a bifurcation of the original symmetric saddle period-one orbit (C^0) at the base of which the attractor was formed. This bifurcation can be either period-doubling bifurcation (at weak coupling) or the symmetry breaking bifurcation (at strong coupling). Then, with the change in the coupling parameter the period-doubling bifurcations of other symmetric saddle orbits $2^N C^0$ originating from C^0 enforce the bubbling phenomenon. With further change in the coupling parameter the riddled basin is observed in the system. The holes from basins of another attractor located outside the symmetric subspace penetrate into the basins of the symmetric chaotic attractor at an arbitrary small distance from the subspace. Then these regions grow and at some critical coupling the system makes a transition to the unsynchronous regime from almost all initial points.

Therefore in the symmetrically coupled logistic maps the saddle periodic orbits of the main family, which form the skeleton of the chaotic attractor, play an important role in the bifurcational mechanism of the chaotic synchronization loss. The first bifurcations of these orbits take place in the symmetric subspace and form the chaotic attractor, the second bifurcations of the same orbits take place transversal to the symmetric subspace (the eigenvector associated with the largest multiplier is in the transversal direction to the symmetric subspace), and they lead to destruction of synchronous chaos.

If these second bifurcations take place before the transition to chaos, at weak coupling (when they occur with stable orbits), they lead to the increase in the number of cycles in the phase space and, therefore, to the formation of multistability in the system [13].

Does a connection between the bifurcation mechanisms of the loss of chaos synchronization and the formation of the multistability exist? Is this situation typical for different symmetrically coupled oscillators with period doubling or is it a peculiarity of the coupled logistic maps? To answer these questions, we consider a more general model of the coupled Hénon maps and perform a detailed bifurcational analysis of the main family of periodic orbits appearing as a result of the subharmonic cascade. We find that the overall behavior of the Henon map, though more complex and invertible, is very similar to the one for the logistic map. In this

paper, it is shown that the multistability formation and the loss of chaotic synchronization turn out to be two facets of the common bifurcational mechanism. The phenomena of bubbling, riddling transition, and multistability observed in coupled Hénon maps are expected to exist in real physical period doubling systems described by invertible differential equations.

II. DYNAMICS OF COUPLED HÉNON MAPS

We study dynamics of the coupled Hénon maps of the form

$$\begin{aligned} x_1(n+1) &= \lambda_1 - x_1^2(n) + y_1(n) \\ &\quad + \epsilon\{x_1^2(n) - x_2^2(n) + y_2(n) - y_1(n)\}, \\ y_1(n+1) &= b x_1(n), \\ x_2(n+1) &= \lambda_2 - x_2^2(n) + y_2(n) \\ &\quad + \epsilon\{x_2^2(n) - x_1^2(n) + y_1(n) - y_2(n)\}, \\ y_2(n+1) &= b x_2(n), \end{aligned} \tag{1}$$

where $x_{1,2}(n), y_{1,2}(n)$ are dynamical variables of the system, $\lambda_{1,2}, b$ are parameters of each individual map, ϵ is a coupling coefficient. The coefficient b can be interpreted as the parameter of the dissipation of the system.

This type of interaction between individual systems corresponds to the future coupling. When $b=0$ the system (1) reduces to the coupled logistic maps. If $b \neq 0$ the system becomes invertible.

We investigate the dynamics of identical maps (1) ($\lambda_1 = \lambda_2 = \lambda$) at fixed $b=0.3$ depending on the parameters λ and ϵ in the intervals [0; 1.25] and [0; 0.5], respectively. The case of mismatched subsystems will be considered later.

In $0 < \lambda < 0.3675$ the system (1) has a stable fixed point C^0 located in the symmetric subspace $x_1 = x_2$, $y_1 = y_2$ for all considered values of the coupling coefficient. As λ increases, a set of period-doubling bifurcations of symmetric periodic orbits $2^N C^0$ ($N=0,1,2,\ldots$) takes place on the base of the point C^0. The lines of these bifurcations are displayed in Fig. 1, which demonstrates bifurcations of regimes in the symmetric subspace. For ϵ on the right side of the line l_{b1}, a cascade of bifurcations leads to formation of a chaotic attractor located in the symmetric subspace. With a further increase in λ, the stability windows for orbits with different periods are created through the saddle-node bifurcations. Figure 1 shows the stability windows only for two orbits with equal periods ($7C_1^0, 7C_2^0$), which have the largest regions of existence in the parameter plane. As λ increases, a cascade of the period-doubling bifurcations takes place on the base of these orbits. As a result chaotic attractors $7A_1^0$ and $7A_2^0$ are formed.

Regimes of regular synchronous motions are observed at all values of ϵ. The regime of chaotic synchronous motions exists only in the limited region in ϵ. As the coupling coefficient decreases, the loss of the transversal stability turns it into the out-of-phase regime. As the line l_{b1} is crossed, the transitions to different unsynchronous regimes are observed depending on λ. As ϵ is further decreased, chaotic attractors A^0, $2A^0$, $4A^0$, $8A^0$ are changed by stable orbits $2C^1$, $4C^2$ (or $8C^4$), $8C^4$, and $16C^8$, respectively. The chaotic attractors $7A_1^0$ and $7A_2^0$ are changed into orbits $14C_1^7$ and $14C_2^7$. Projections of phase portraits in the out-of-phase regimes are presented in Fig. 2, which show symmetric orbits.

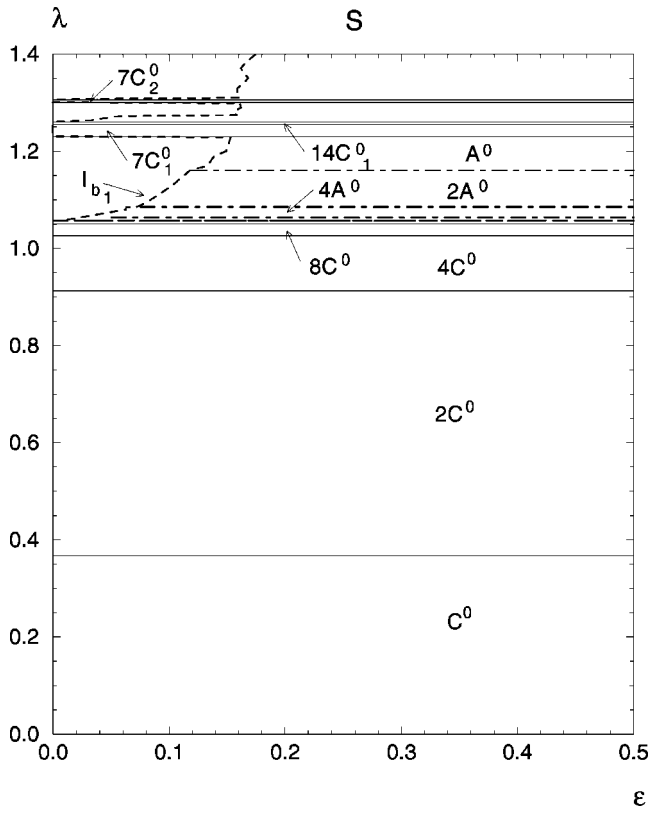

FIG. 1. Regions of the existence of regular and chaotic synchronous regimes in the plane of the control parameters (sheet S).

The transition from the synchronous chaos to the out-of-phase regular regimes occurs analogous to the one for the coupled logistic maps [10]. Let us consider the transition from the synchronous chaotic attractor to the out-of-phase regime $2C^1$ at $\lambda = 1.2$ in more detail. Figure 3 shows the time series $[x_1(n) - x_2(n)]$ in a slightly mismatched system ($\lambda_1 = \lambda$, $\lambda_2 = \delta\lambda$, $\delta = 0.995$). Note that the destruction of chaotic synchronization begins with the bubbling behavior. The bubbling of the attractor becomes visible for $\epsilon < 0.2$. For larger ϵ the parameter mismatch does not sufficiently influence the synchronous regime. From the figure it is seen that the intermittency becomes more developed as the coupling coefficient decreases. The bubbling behavior is observed in the interval of ϵ between 0.2 and 0.15. Then the system makes a transition to the stable orbit $2C^1$ [see Fig. 3(d)]. For exactly identical maps ($\delta = 1$), the dynamical behavior of the system depends on the initial values in a complex manner at this value of ϵ. The small change in initial conditions leads to situations where the phase trajectory is attracted either to the symmetric chaotic set A^0 or to the periodic orbit $2C^1$. Figure 4 shows two time series $(x_1 - x_2)$ for the same

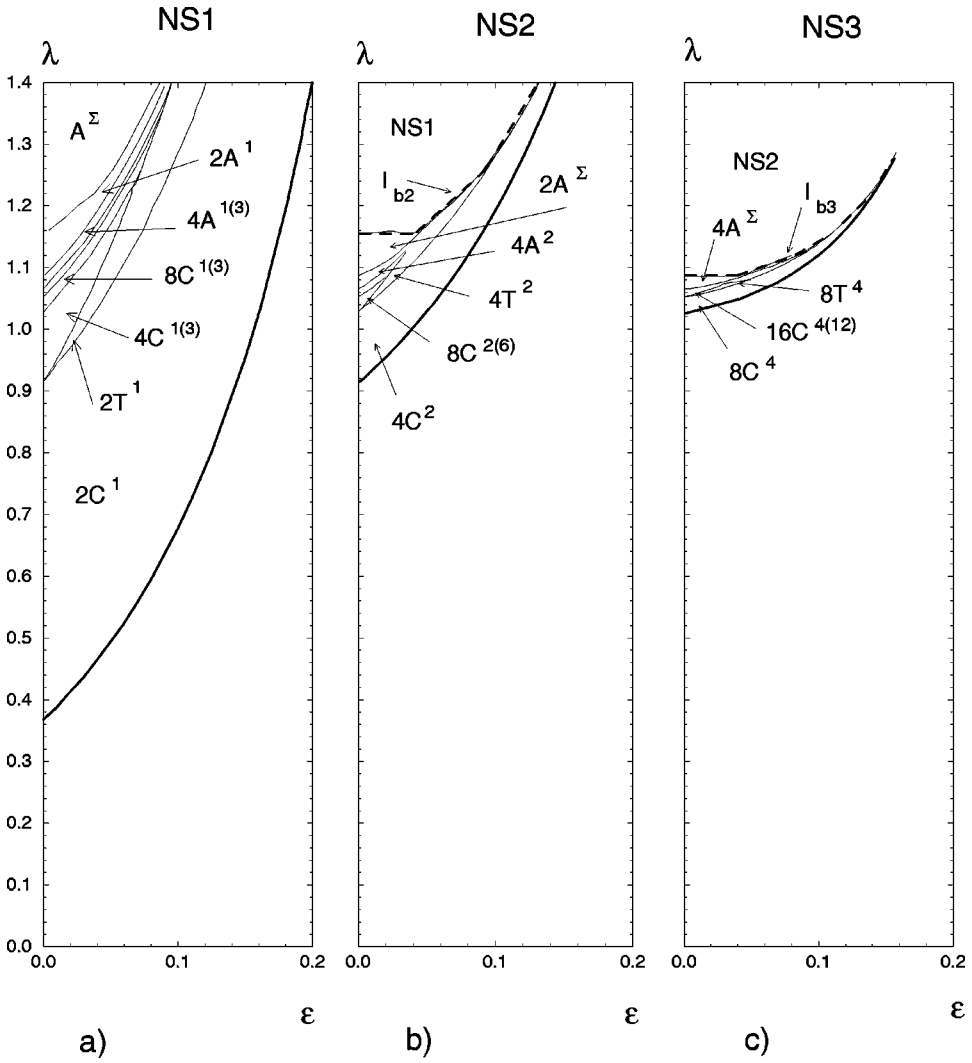

FIG. 2. Regions of the existence of unsynchronous regimes in the plane of the control parameters (sheets NS1, NS2, NS3).

parameters but with nearly initial values, illustrating this phenomenon. The entrance of the phase trajectory into the stable orbit $2C^1$ does not depend on the distance between the initial conditions and the chaotic set A^0. In an arbitrary small neighborhood of the symmetric subspace, it is possible to find initial values, starting from which the phase point heads towards the orbit $2C^1$. This behavior, as will be demonstrated further, is caused by the phenomenon of the riddled basins of the chaotic attractor A^0. With further decrease in ϵ, the regime of chaotic synchronization is not observed. Practically at any initial values from a neighborhood of the set A^0 the phase trajectory heads towards the stable orbit $2C^1$.

At values of λ corresponding to other symmetric chaotic attractors ($2A^0$, $4A^0$, $7A^0$, etc.) the process of the chaotic synchronization loss takes place similarly, but leads to the transition to other unsynchronous regimes mentioned above (Fig. 2). As the control parameter is changed, each orbit gives birth to its own family of out-of-phase regimes. Let us consider oscillating regimes which are formed on the base of stable periodic orbits $2C^1$, $4C^2$, and $8C^4$. Figure 5(a) shows regions of the existence of regimes which are formed on the base of $2C^1$ [Fig. 2(a)]. Projections of the phase portraits of typical regimes are presented in Fig. 6. As the control parameter is changed, the stable orbit $2C^1$ is softly changed by quasi-periodic oscillations $2T^1$ [Fig. 6(a)]. For large λ we observe a transition to chaos through the tori breaking mechanism as the coupling is decreased. For small λ either a stable periodic orbit $4C^1$ [Fig. 6(b)] or another stable periodic orbit $4C^3$ [Fig. 6(c)] appears as ϵ decreases. These orbits coexist and are symmetric with respect to each other under $x_1 \leftrightarrow x_2$, $y_1 \leftrightarrow y_2$. As λ increases, a cascade of period-doubling bifurcations occurs on the base of both of these orbits, which ends with the appearance of chaos. In the region of chaos a sequence of boundary-crisis bifurcations is observed, which is accompanied by the merging of the chaotic sets. Figures 6(d) and 6(e) show projections of phase portraits of coexisting chaotic attractors $4A^1$ and $4A^3$, which are formed on the base of the orbits $4C^1$ and $4C^3$, respectively. As the control parameter is changed, these chaotic sets merge and eventually a chaotic attractor $2A^1$ [Fig. 6(f)] appears to end the evolution of this family. Afterwards, a chaotic attractor A^Σ [Fig. 6(g)], which contains chaotic sets of different families, completes the development of the synchronous chaos in the system.

Figures 5(b) and 5(c) show maps of out-of-phase regimes for two other families. As the control parameter is changed,

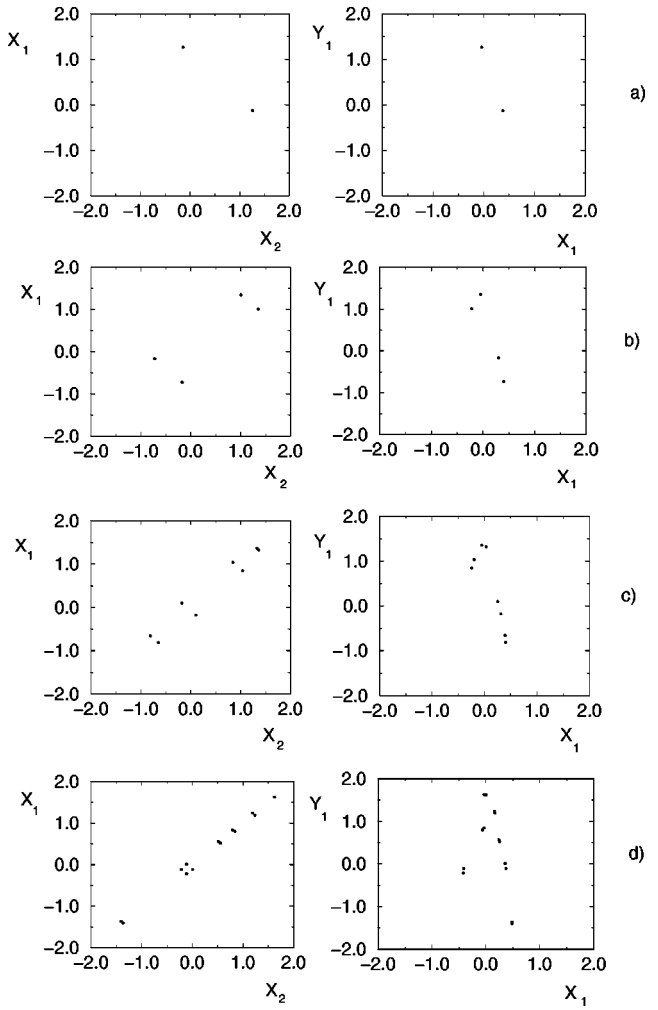

FIG. 3. Projections of the phase portraits in the out-of-phase regimes, which appear after the breakup of chaotic synchronization [(a) $2C^1$, (b) $4C^2$, (c) $8C^4$, (d) $14C_1^7$].

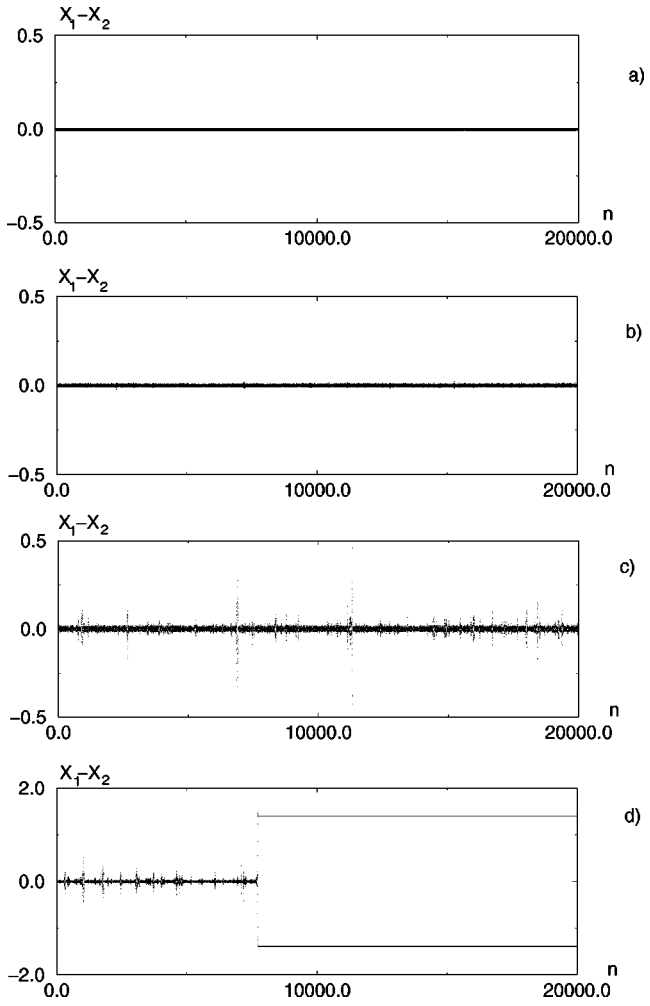

FIG. 4. Time series of the difference of dynamical variables which illustrate the process of the loss of chaotic synchronization [$\lambda=1.2$, $\delta=0.995$, $\epsilon=0.25(a)$, $0.19(b)$, $0.16(c)$, $0.15(d)$].

the orbits $4C^2$ and $8C^4$ are created and the transitions similar to ones on the base of $2C^1$ occur. However, these families occupy smaller regions in the parameters plane. In the figure the boundaries of the sheets are shown in thick lines. The sheets $NS2$ and $NS3$ of families of unsynchronous regimes are bound by the lines l_{b2} and l_{b3} [Figs. 5(b),5(c)]. As these lines are crossed, the system jumps from one family of regimes to another one. Unsynchronous oscillations on the base of $8C^4$ turn into regimes on the base of $4C^2$, which in turn becomes ones on the base of $2C^1$. Projections of the phase portraits for several main regimes on the sheets $NS2$ and $NS3$ are presented in Figs. 7 and 8. Evolution of the family of the regimes on the base of $8C^4$ leads to the chaotic attractor $8A^4$ [Fig. 8(c)]. Next there is a transition to the attractor $4A^{\Sigma}$ [Fig. 8(d)], which includes the chaotic set $8A^4$ and chaotic sets of other families (for example, ones formed on the base of the orbit $16C^8$). Evolution of regimes formed on the base of $4C^2$ (the sheet $NS2$) is completed by the appearance of the chaotic attractor $4A^2$ [Fig. 7(c)]. Then there occurs a transition to the attractor $2A^{\Sigma}$, which includes the chaotic sets $4A^2$ and $4A^{\Sigma}$.

The comparison of the maps of regimes in Figs. 1 and 5 shows that there are regions in the parameters plane where the sheets S, $NS1$, $NS2$, and $NS3$ overlap. In the phase space, the attractors for different families coexist simultaneously. The region of multistability is bounded by the boundary of the sheet $NS1$. The maximum number of coexisting attractors is observed at small coupling in a neighborhood of the chaos transition for the individual oscillator (λ_c). At $\lambda<\lambda_c$ these attractors become regular ones. At $\lambda>\lambda_c$ one can find both regular and chaotic attractors depending on initial conditions. The set of coexisting states depends on the value of ϵ.

Thus, phenomena of synchronization and multistability are observed in the coupled Hénon map system (1). The loss of chaos synchronization is accompanied by bubbling and riddling transitions, leading to the appearance of a stable periodic orbit, which gives birth to its own family of typical regimes. The comparison of maps of the several dynamical regimes shows that the higher the period of the orbit on the base of which a family of out-of-phase regimes is formed, the smaller the regions which it occupies in the parameters plane.

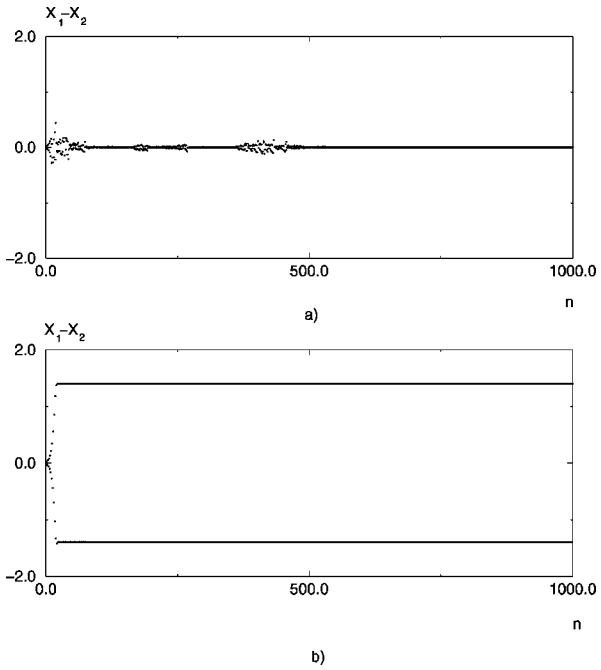

FIG. 5. Time series of the difference of dynamical variables at equal values of the parameters ($\lambda=1.2$, $\epsilon=0.15$) and close initial points [(a)$x_1(0)=0.795$, $x_2(0)=0.804$, $y_1(0)=0.245$,$y_2(0)=0.236$; (b)$x_1(0)=0.795$, $x_2(0)=0.805$, $y_1(0)=0.245$, $y_2(0)=0.235$].

III. BIFURCATIONAL ANALYSIS OF LOSS OF CHAOTIC SYNCHRONIZATION AND FORMATION OF MULTISTABILITY

In this section we investigate mechanisms of the complete chaotic synchronization loss and multistability formation in the coupled Hénon maps (1). We consider the case of identical subsystems when $\lambda_1=\lambda_2=\lambda$. Figure 9 shows bifurcational lines for the main family of symmetric orbits 2^NC^0 in the plane of the control parameters $\epsilon-\lambda$. On lines l_s^i (i is the period of the orbit) one of the multipliers of the orbits becomes -1. The symmetric orbits lose their stability under perturbations within the symmetric subspace but remain stable under transversal perturbations. Stable periodic orbits with doubled periods appear in their neighborhood within the symmetric subspace. Thus in the symmetric subspace a cascade of period-doubling bifurcations takes place, where a chaotic attractor is formed. As a result, on the right side of the line l^1 there is a transition to synchronous chaotic attractors 2^NA^0 as λ increases. On the lines l_t^i the saddle orbits 2^NC^0 in the symmetric subspace undergo period-doubling bifurcations, which become unstable in the transversal direction as well. In their neighborhoods the saddle orbits with doubled periods appear outside the symmetric subspace: for example, $C^0\rightarrow 2C^1$, $2C^0\rightarrow 4C^2$, $4C^0\rightarrow 8C^4$ on lines l^1, l^2, l^4, respectively. As ϵ decreases these out-of-phase orbits become stable as the bifurcational lines l_r^2, l_r^4, l_r^8 are crossed.

Let us consider the process of a loss of chaos synchronization in more detail. On the right side of the line l^1 (Fig. 9) for $\lambda=1.2$ the one-band symmetric chaotic attractor A^0 exists in the phase space. The regime of chaos synchronization is stable and robust. The saddle symmetric orbits 2^NC^0 embedded in the chaotic attractor are stable under transversal perturbations. With the decrease in ϵ the saddle point C^0 loses its transversal stability at the line l^1, producing the saddle orbit $2C^1$ outside the symmetric subspace. This bifurcation induces the bubbling behavior in the system, which is observed between the lines l_t^1 and l_p^2. The regime of chaotic synchronization becomes not robust. As the coupling coefficient is decreased further, the orbit $2C^1$ undergoes a pitchfork bifurcation on the line l_p^2 ($\epsilon=0.18$). In its neighborhood, a pair of saddle period-2 orbits, which are symmetric with respect to each other, appear and the orbit $2C^1$ becomes stable. In the system of coupled logistic maps [10] it was shown that a similar bifurcation leads to the riddling of the basin.

In order to investigate the structure of the basins of A^0, Eqs. (1) are rewritten in new variables

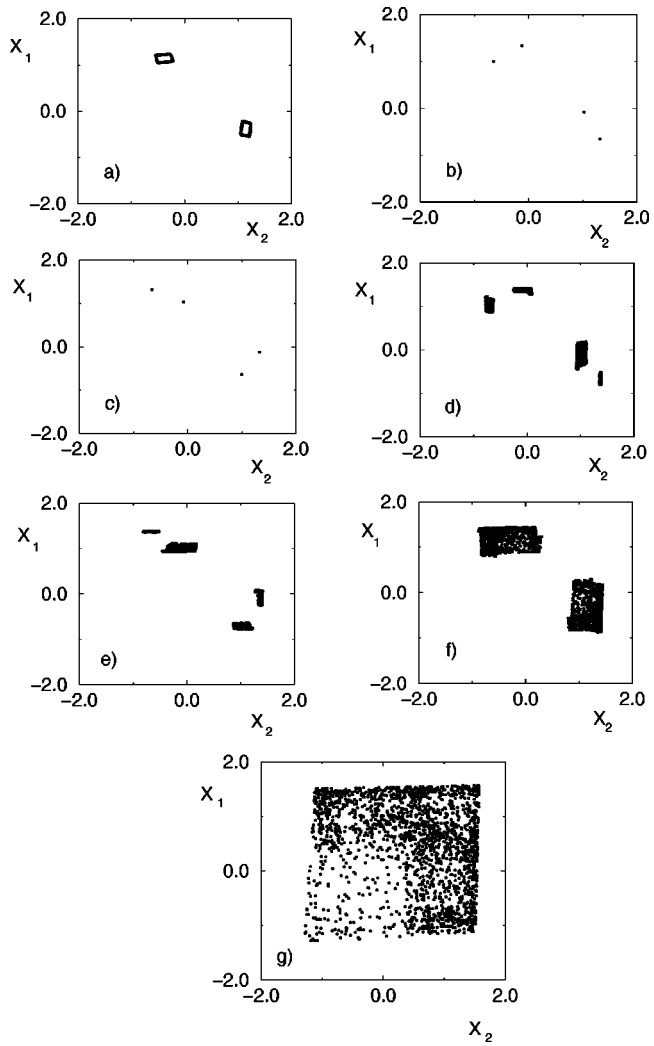

FIG. 6. Projections of the phase portraits of typical regimes from the base of the orbit $2C^1$: (a) $2T^1$, (b) $4C^1$, (c) $4C^3$, (d) $4A^1$, (e) $4A^3$, (f) $2A^1$, (g) A^Σ.

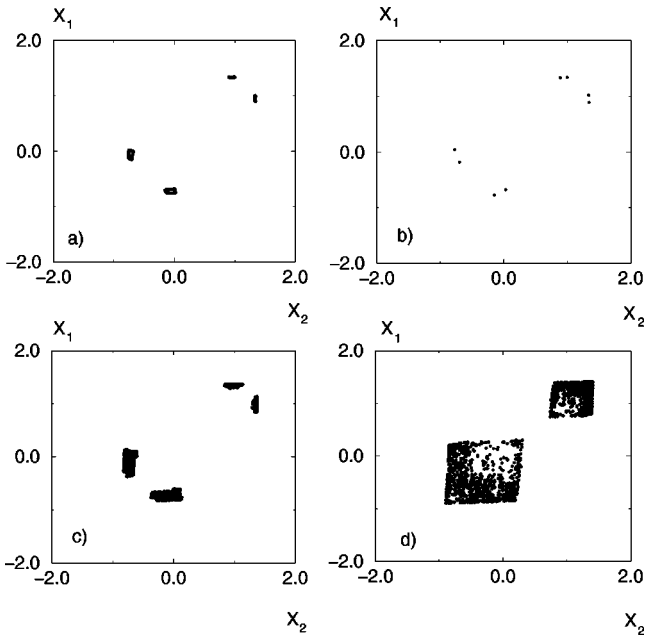

FIG. 7. Projections of the phase portraits of typical regimes from the base of the orbit $4C^2$: (a) $4T^2$, (b) $8C^4$, (c) $4A^2$, (d) $2A^{\Sigma}$.

$$
\begin{aligned}
s(n+1) &= -2s(n)u(n) + r(n) + 2\epsilon[2s(n)u(n) - r(n)], \\
r(n+1) &= bs(n), \\
u(n+1) &= \lambda - u(n)^2 - s(n)^2 + v(n), \\
v(n+1) &= bu(n),
\end{aligned}
\tag{2}
$$

where

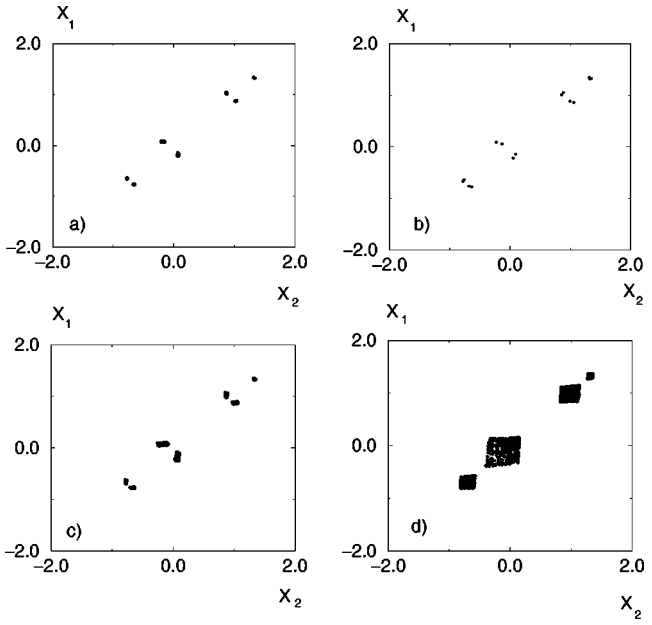

FIG. 8. Projections of the phase portraits of typical regimes from the base of the orbit $8C^4$: (a) $8T^4$, (b) $16C^8$, (c) $8A^4$, (d) $4A^{\Sigma}$.

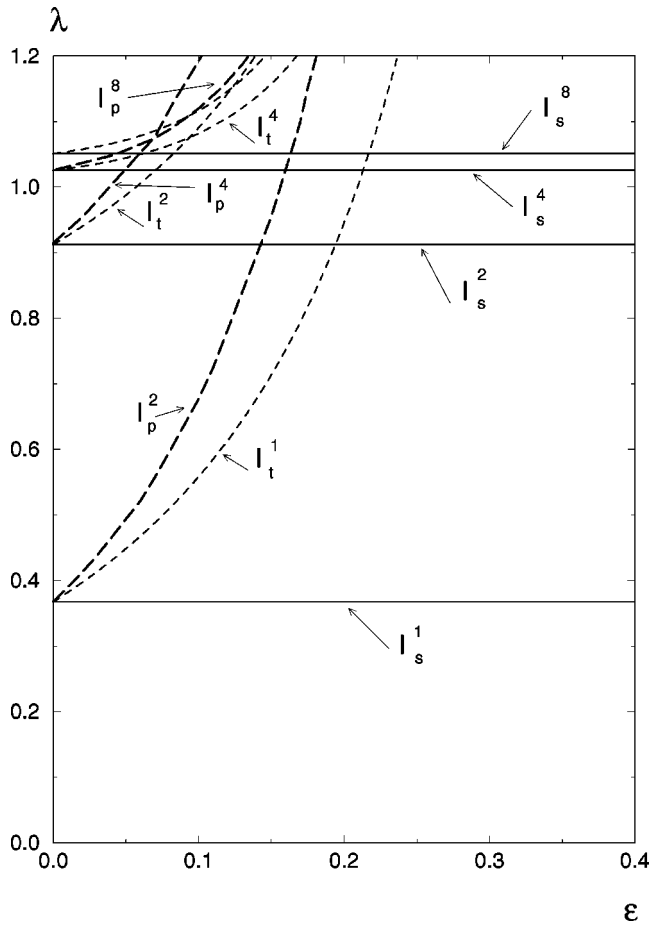

FIG. 9. Bifurcational lines of periodic orbits of the main family in the parameter plane.

$$
s = \frac{x_1 - x_2}{2}, \quad r = \frac{y_1 - y_2}{2},
$$

$$
u = \frac{x_1 + x_2}{2}, \quad v = \frac{y_1 + y_2}{2}.
$$

In the case of synchronous motions, $s=0$ and $r=0$, so that the state of the system is characterized by the dynamical variables u and v in the two-dimensional symmetric subspace. We obtain the section of basins of the chaotic attractor A^0 and of the stable orbit $2C^1$ on the plane (s,r) at fixed values of u and v.

Figure 10 shows the sections of basins for a set of ϵ when u and v are chosen to be at the fixed point C^0. In this section, C^0 is located at the origin, that is, $s=0, r=0$. Figure 10 shows that after the bifurcation of $2C^1$ it becomes stable and in a small vicinity of the saddle point C^0 embedded in the chaotic attractor A^0 there exist phase trajectories that are attracted to the orbit $2C^1$. However, when the value of the parameter is close to the bifurcation point [Fig. 10(a) corresponds to $\epsilon=0.177$] an arbitrary transversal perturbation of the trajectory in a small neighborhood of C^0 does not induce a transition to the orbit $2C^1$. For such transition the perturbations must be along a particular direction in the two-dimensional normal subspace (s,r). The farther the parameter is from the critical value, the larger the size of the region

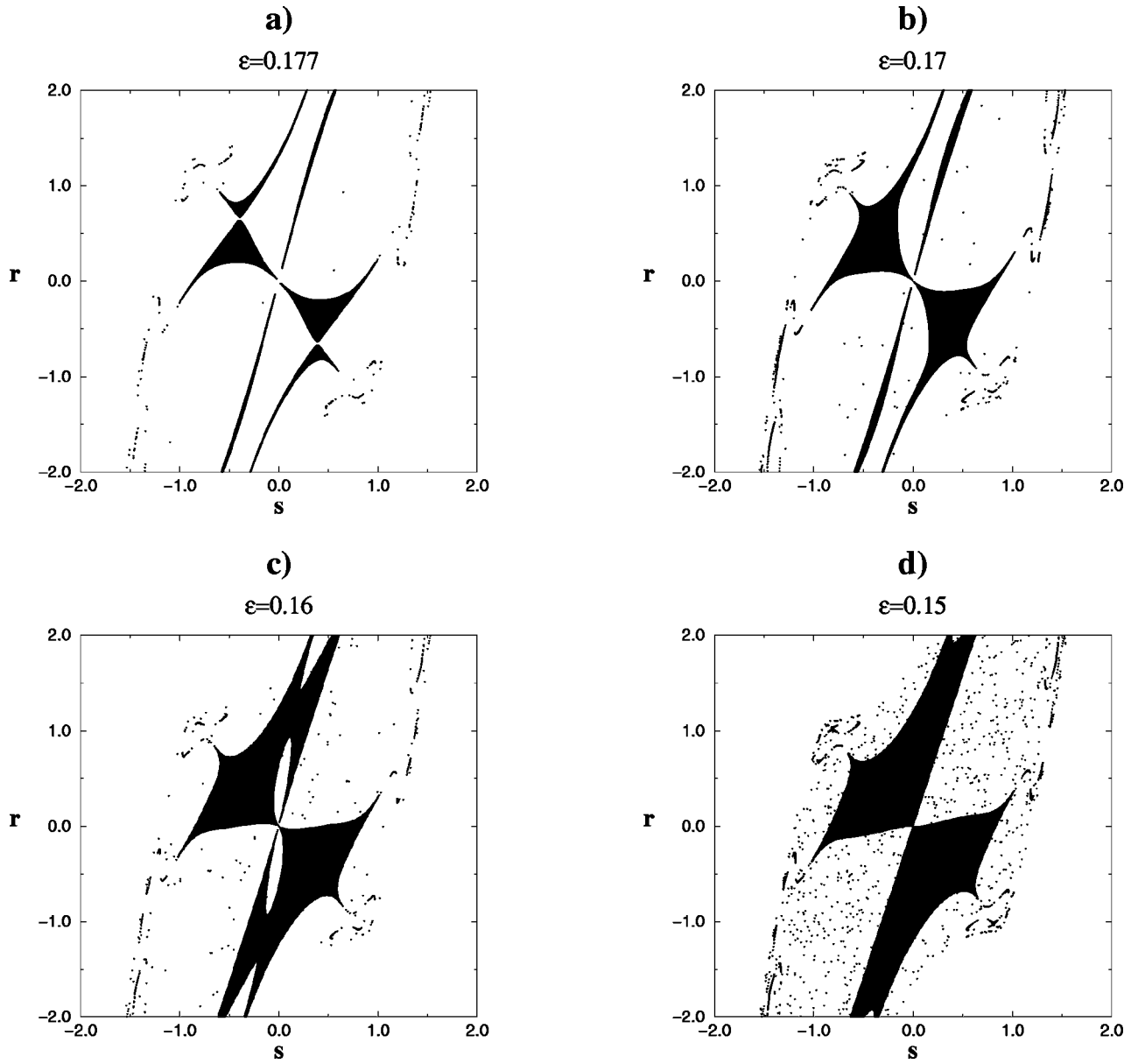

FIG. 10. A section of the basins of the symmetric chaotic attractor (white) and of the stable periodic orbit $2C^1$ (black) as the coupling is decreased. The two other variables are chosen to be at the point C^0.

of initial points near C^0, starting from which the phase trajectory heads towards the stable orbit $2C^1$ [see Figs. 10(a)–10(d)]. For example, at $\epsilon=0.15$ [Fig. 10(d)] there is a wide sector of directions for such transversal perturbations.

Figure 11 shows sections of the basins of A^0 and $2C^1$ for the same values of ϵ but with u and v chosen to be at an arbitrary point in the chaotic attractor. In the figures this point is at the origin, $s=0$, $r=0$. From Fig. 11(a) it is seen that near the bifurcational point ($\epsilon=0.177$) a small vicinity of some points on the attractor is not riddled by holes belonging to the basins of $2C^1$. With further decrease in ϵ the structure of the section of the basins becomes more complex. Points from the basins of $2C^1$ appear in the vicinity of the symmetric subspace in increasing numbers. Figure 11(d) shows the section for $\epsilon=0.15$, where the riddling becomes visible. Similar results hold for other sections of the basins of the attractors. We chose 10 arbitrary points on the attractor and investigated sections of the basins on the plane (r,s). As the coupling coefficient is changed, the rebuilding of the basins occurs similar to these sections.

IV. CONCLUSION

In the coupled Hénon maps, the process of the loss of complete synchronization and the formation of multistability arise from the single bifurcational mechanism. These scenarios are determined by bifurcations of the main family of the saddle periodic orbits 2^NC^0 which form a skeleton of the attractor. The synchronization loss begins with the second period-doubling bifurcation of the orbit C^0: $C^0\rightarrow 2C^1$, after which the regime of chaotic synchronizations becomes

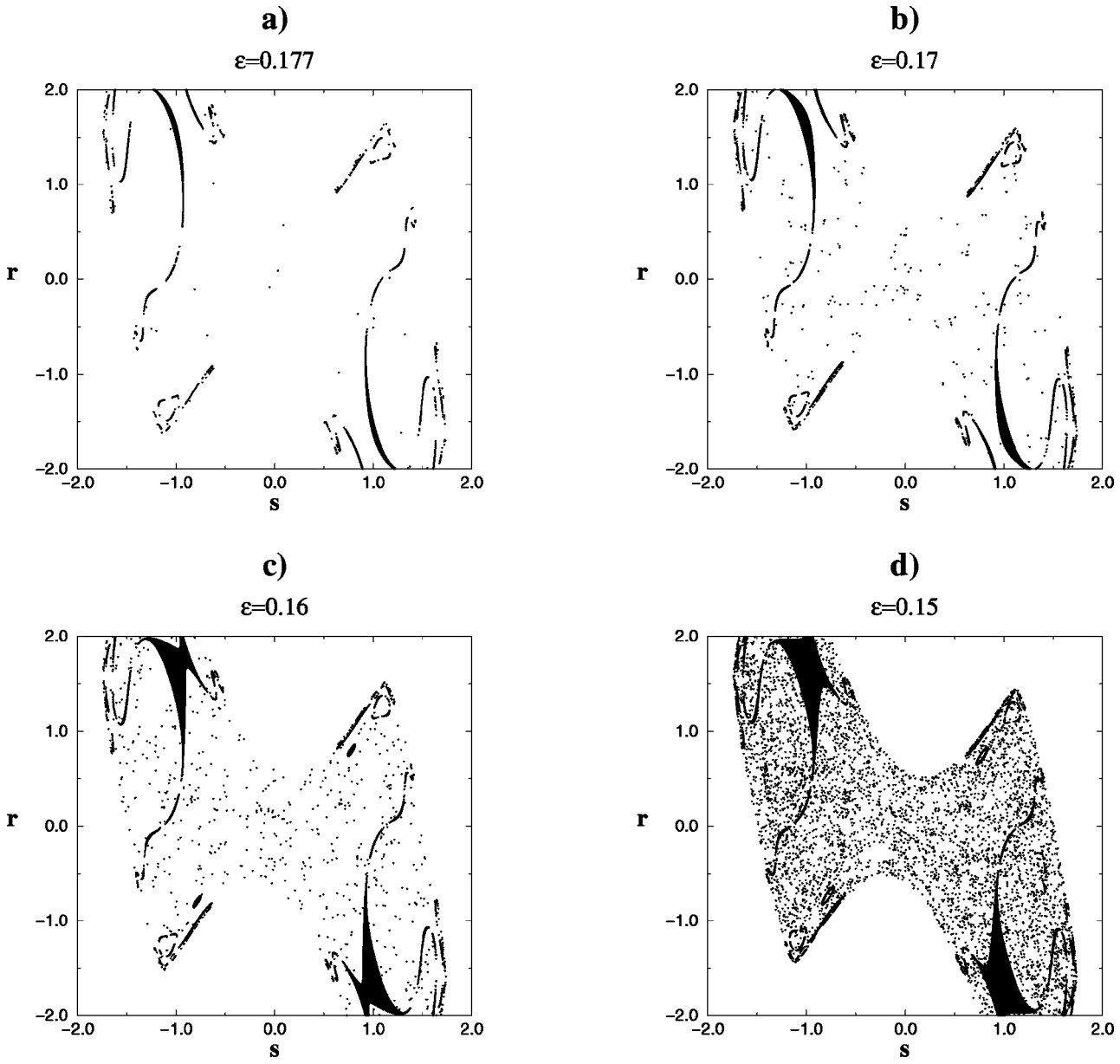

FIG. 11. A section of the basins of the symmetric chaotic attractor (white) and of the stable periodic orbit $2C^1$ (black) as the coupling is decreased. The two other variables are chosen be an arbitrary point in the attractor.

less robust. The second period-doubling bifurcations of the other orbits of the main family 2^NC^0: $2^NC^0 \rightarrow 2^{N+1}C^N$ enforce the bubbling behavior of the attractor. The bifurcation of the saddle orbit $2C^1$ located outside the symmetric subspace leads to formation of the complex structure of the basins of A^0. The vicinity of the chaotic set A^0 becomes riddled by holes from which the phase trajectory leaves towards the orbit $2C^1$. The bifurcations of the other orbits $2^{N+1}C^N$ from 2^NC^0 located outside the symmetric subspace enforce the riddling of the basins of A^0, where holes from basins of the other orbits appear. The attractor A^0 gradually loses its basins and the regime of nonrobust chaotic synchronization is gradually destroyed.

At weak coupling the same bifurcations of the orbits lead to multistability in the system. The first step is the second period-doubling bifurcations of the in-phase orbits 2^NC^0 which lead to the increase in number of coexisting saddle orbits in the phase space of the system. The second step is the bifurcations of out-of-phase orbits $2^{N+1}C^N$, which turn these orbits into stable ones.

The bifurcational mechanism in the coupled Hénon maps (1) is very similar to the ones in the coupled logistic maps [10]. But it has some differences. Namely, the riddling of the basins does not appear immediately after the bifurcation of the saddle orbit $2C^1$. The complication of the structure of the basins occurs gradually with leaving of the parameter from the bifurcational point. This peculiarity may be due to the higher dimensionality of the system (1). In a model of coupled oscillations with minimal dimension ($n=2$) after the bifurcation of $2C^1$ any transversal perturbation in a neighborhood of C^0 induces a transition to the out-of-phase regime. In the coupled Hénon maps, this takes place only

when the perturbations have a well-defined direction.

In noninvertible systems the so-called pre-images play an important role in the loss of complete synchronization [7,9]. The investigation of the invertible system shows that the existence of the preimages is not a necessary condition for phenomena of bubbling behavior and riddled basins. This point is important since real physical systems are described by invertible differential equations and, therefore, the phenomena described in our work can occur in such systems.

ACKNOWLEDGMENTS

We acknowledge the support by Award No. REC-006 of the U.S. Civilian Research & Development Foundation for the Independent States of the Former Soviet Union (CRDF) and the Naval Research Laboratory under Contract No. N68171-00-M-5430. We also thank the Korean Ministry of Education and the Korean Ministry of Science and Technology for support. V. Asktakhov acknowledges support by the NCSL at POSTECH during his visit.

[1] H. Fujisaka and T. Yamada, Prog. Theor. Phys. **69**, 32 (1983).
[2] V. S. Afraimovich, N. N. Verichev, and M. I. Rabinovich, Radiophys. Quantum Electron. **29**, 795 (1986).
[3] N. F. Rulkov, M. M. Sushchik, L. S. Tsimring, and H. D. I. Abarbanel, Phys. Rev. E **51**, 980 (1995).
[4] V. S. Anishchenko, T. E. Vadivasova, and D. E. Postnov, Int. J. Bifurcation Chaos Appl. Sci. Eng. **2**, 633 (1992).
[5] M. G. Rosenblum, A. S. Pikovsky, and J. Kurths, Phys. Rev. Lett. **76**, 1804 (1996).
[6] A. S. Pikovsky and P. Grassberger, J. Phys. A **24**, 4587 (1991).
[7] P. Ashwin, J. Buescu, and I. Stewart, Phys. Lett. A **193**, 126 (1994).
[8] P. Ashwin, J. Buescu, and I. Stewart, Nonlinearity **9**, 703 (1996).
[9] Y. C. Lai, C. Grebogi, J. A. Yorke, and S. C. Venkataramani, Phys. Rev. Lett. **77**, 55 (1996).
[10] V. Astakhov, A. Shabunin, T. Kapitaniak, and V. Anishchenko, Phys. Rev. Lett. **79**, 1014 (1997).
[11] V. Astakhov, M. Hasler, T. Kapitaniak, A. Shabunin, and V. Anishchenko, Phys. Rev. E **58**, 5620 (1998).
[12] M. M. Sushchik, N. E. Rulkov, and H. D. I. Abarbanel, IEEE Trans. Circuits Syst. **44**, 866 (1997).
[13] V. V. Astakhov, B. P. Bezruchko, E. N. Erastova, and E. P. Seleznev, JETP **60**, 19 (1990).